Pergamon

Int. J. Heat Mass Transfer. Vol. 40, No. 16, pp. 3955–3967, 1997

Printed in Great Britain
0017–9310/97 $17.00+0.00

PII: S0017-9310(97)00008-2

Natural convective heat transfer in a fluid saturated variable porosity medium

P. NITHIARASU, K. N. SEETHARAMU and T. SUNDARARAJAN
Department of Mechanical Engineering, Indian Institute of Technology, Madras 600 036, India

(*Received* 20 *October* 1995 *and in final form* 5 *November* 1996)

Abstract—A generalised non-Darcian porous medium model for natural convective flow has been developed taking into account linear and non-linear matrix drag components as well as the inertial and viscous forces within the fluid. The results of the general model have been validated with the help of experimental data and compared with the various non-Darcy porous media model predictions reported in literature. It has been observed that the wall Nusselt number is significantly affected by the combination of dimensionless parameters such as Rayleigh number, Darcy number and porosity in the non-Darcy flow regime. A detailed parametric study has been presented for natural convective flow inside a rectangular enclosure filled with saturated porous medium of constant or variable porosity. It is observed that the thickness of the porous layer and the nature of variation in porosity significantly affect the natural convective flow pattern as well as the heat transfer features. The present model is also able to predict the channeling effect and associated heat transfer in forced flow through packed beds. © 1997 Elsevier Science Ltd.

1. INTRODUCTION

Flows through porous media occur in a wide variety of applications such as geothermal energy systems, secondary and tertiary oil recovery, prevention of subsoil water pollution, etc. In recent times, porous media models are also being applied for simulating more generalised situations such as flow through packed and fluidized beds, liquid metal flow through dendritic structures in alloy casting and even for obtaining approximate solutions for flow through turbomachinery. Some of these problems involve contiguous regions of fluid and porous medium. In order to analyse such emerging applications, it is necessary to consider porous media models which are applicable over a wide porosity range. In the present work, a generalised porous medium model which reduces to the Navier–Stokes equations for porosity equal to 1 and to the earlier porous media models in the appropriate ranges of parameters, is presented. The validity of this model is investigated by studying the buoyancy driven flow in a two-dimensional rectangular cavity and comparing the results with those of earlier studies. The present model has also been applied for forced convective heat transfer through a variable porosity medium and compared with the experimental data available in literature. A detailed parametric study has been carried out for natural convective flow in a free fluid surrounded by a saturated porous medium of variable porosity.

Free convective heat transfer in a porous medium has been studied widely in literature. Cheng [1] provides an extensive review of literature on free convection in fluid saturated porous media with regard to applications in geothermal systems. Nield and Bejan [2] given an excellent summary of the subject. Regarding porous media models, the phenomenological relation between the pressure drop across a saturated porous medium and the flow rate was first established by Darcy (1856). Several authors have since used the Darcy's relation or its modified forms, for modelling a variety of porous media flows [3–10]. Two notable modifications of Darcy's law are the Brinkman's (1947) and the Forchheimer's (1901) extensions which account for the viscous stresses adjacent to the bounding walls and the non-linear drag effect due to the solid matrix respectively. Even though these models have been widely used by many authors [1–10], they are not general enough to be applicable for a medium with variable porosity. In particular, they do not reduce to the free fluid case when porosity is 1. In recent years, some authors have considered a modified form of the Navier–Stokes equations including all fluid forces and the solid matrix drag in the momentum equations. In this respect, Vafai and Tien [11] have established the steady-state governing equations for a porous medium using the local volume averaging technique. They represented the drag forces on the solid matrix through the Ergun's relation [12] and applied their formulation of the flow through a porous medium over a flat surface. Lage [13] employed a similar formulation and obtained an approximate correlation for the Nusselt number using scale analysis, for a natural convective flow inside a rectangular cavity. While the usage of Ergun's relation for representing the non-linear solid matrix drag is of recent origin [11, 13, 14], a majority of authors have used the Forchheimer's extension.

NOMENCLATURE

A	coefficient of linear term in matrix drag expression
a_f	fraction of flow area available per unit cross-sectional area
B	coefficient of quadratic term in matrix drag expression
c_p	specific heat
Da	Darcy number
Da_w	wall Darcy number
D_p	particle size
D_y	matrix drag per unit volume in y-direction
g	acceleration due to gravity
k_{eq}	equivalent thermal conductivity of the medium
L_{ref}	characteristic dimension
l	thickness of porous medium
p_f	fluid pressure
Pr	Prandtl number
Ra	Rayleigh number
Ra^*	Darcy–Rayleigh number $= (Ra\ Da)$
T	temperature
T_i	initial temperature as well as cold wall temperature
T_w	hot wall temperature
t	non-dimensional time
TR	thickness ratio $= l/L_{ref}$
u	velocity component in x-direction
u_f	fluid velocity in x-direction
$\bar{u}$	volume averaged velocity in x-direction
v	velocity component in y-direction
v_f	fluid velocity in y-direction
$\bar{v}$	volume averaged velocity in y-direction
x, y	coordinate axes.

Greek symbols

α	thermal diffusivity $= k_{eq}/(\rho c_p)_f$
β	coefficient of volumetric thermal expansion
ε	porosity
ε_w	porosity value at wall
κ	permeability
μ_f	fluid viscosity
ν	kinematic viscosity
ρ	density
ρ_f	fluid density
ρ_{ref}	reference density.

Subscripts

f	fluid
ref	reference
w	wall.

Superscript

*	non-dimensional quantities
n	nth time level.

For instance, Lauriat and Prasad [15] and Shin-Wen Hsiao [16] accounted for the non-linear particle drag by the Forchheimer's approach. Investigations of forced convective flow and heat transfer through a variable porosity medium have been carried out by Vafai and coworkers [11, 17–20]. In the present paper, a generalised frame work for natural convective flow through a medium of variable porosity is presented, along with a detailed parametric study of heat transfer and flow in the non-Darcy regime.

2. DEVELOPMENT OF THE GENERALISED VARIABLE POROSITY MODEL

The existing non-Darcy porous medium flow models present a rather confusing picture; some authors employ the fluid velocity components u_f and v_f, while others use the superficial velocity components (u, v). Accordingly, the governing equations of these approaches are not similar. A second source of confusion is the non-dimensionalisation employed for the various quantities. Although most authors take the solid matrix drag in the form of a linear viscous term and a quadratic term representing the inertial drag (loss of kinetic energy), the coefficient values used for these terms differ from author to author. In the present paper, an attempt has been made to develop a general set of governing equations of non-Darcian natural convective flow in a medium of variable porosity. A detailed account of the derivation for the governing equations is also presented, for the sake of completeness.

Consider the balance of mass, momentum and energy for two-dimensional flow in a fluid saturated medium of variable porosity. We shall assume the medium to be isotropic with constant physical properties, except for the non-homogeneous porosity. Let a_f be the fraction of area available for flow per unit cross-sectional area, at a location in a given direction. In fact, a_f is an averaged quantity, the average being taken over the length scale of the voids (or the length scale of the particles, if the porous bed is made up of particles), in the direction perpendicular to the flow area under consideration. For an isotropic porous bed, a_f will be the same in all the directions and it can also be shown to be equal to the local bed porosity, ε.

In spite of averaging over the void length scale, the fractional flow area a_f may vary from location to location on the macro-length scale L_{ref} of the physical problem, due to variation of the bed porosity.

Let us now consider the derivation of the governing equations for a non-homogeneous porous medium. For a control volume of size $(\Delta x \cdot \Delta y \cdot 1)$, the flow area available in the x-direction will be $(a_f \cdot \Delta y \cdot 1)$ for unit depth in z-direction. Denoting the average fluid velocities over the control volume faces in x- and y-directions as u_f and v_f, the mass balance for the control volume is written as

$$(u_f a_f \Delta y)|_{x+\Delta x} - (u_f a_f \Delta y)|_x + (v_f a_f \Delta x)|_{y+\Delta y} - (v_f a_f \Delta x)|_y + \frac{\partial}{\partial t}(\rho_f a_f \Delta x \Delta y) = 0. \quad (1)$$

The porosity ε of the medium can be obtained as

$$\varepsilon = \frac{\text{void volume}}{\text{total volume}} = \frac{a_f \Delta x \Delta y 1}{\Delta x \Delta y 1} = a_f. \quad (2)$$

Defining volume averaged velocity components [2] through the expressions

$$\bar{u} = \varepsilon u_f \quad \text{and} \quad \bar{v} = \varepsilon v_f \quad (3)$$

equation (1) can be simplified for an incompressible flow as

$$\frac{\partial \bar{u}}{\partial x} + \frac{\partial \bar{v}}{\partial y} = 0. \quad (4)$$

Now, let us consider the y-momentum equation including the effect of buoyancy force for the fluid inside the control volume, as shown below:

$$\frac{\partial}{\partial t}(\rho_f v_f a_f \Delta x \Delta y) + (\rho_f u_f v_f a_f \Delta y)|_{x+\Delta x} - (\rho_f u_f v_f a_f \Delta y)|_x + (\rho_f v_f^2 a_f \Delta x)|_{y+\Delta y} - (\rho_f v_f^2 a_f \Delta x)|_y$$
$$= \left(-p_f + 2\mu_f \frac{\partial v_f}{\partial y}\right) a_f \Delta x|_{y+\Delta y} - \left(-p_f + 2\mu_f \frac{\partial v_f}{\partial y}\right) a_f \Delta x|_y + \mu_f \left(\frac{\partial u_f}{\partial y} + \frac{\partial v_f}{\partial x}\right) a_f \Delta y|_{x+\Delta x} - \mu_f \left(\frac{\partial u_f}{\partial y} + \frac{\partial v_f}{\partial x}\right) a_f \Delta y|_x - (\rho_f - \rho_{ref}) g a_f \Delta x \Delta y - \hat{D}_y. \quad (5)$$

Here, $\hat{D}_y$ is the drag due to the solid matrix in y-direction and ρ_{ref} is the reference fluid density. Using equation (3), the above expression can be simplified as

$$\frac{\rho_f}{\varepsilon}\left[\frac{\partial}{\partial t}(\bar{v}) + \frac{\partial}{\partial x}\left(\frac{\bar{u}\bar{v}}{\varepsilon}\right) + \frac{\partial}{\partial y}\left(\frac{\bar{v}^2}{\varepsilon}\right)\right] = -\frac{1}{\varepsilon}\frac{\partial}{\partial y}(p_f \varepsilon) + \frac{\mu_f}{\varepsilon}\nabla^2 \bar{v} + (\rho_{ref} - \rho_f) g - D_y \quad (6)$$

where D_y is the matrix drag per unit volume of the porous medium.

Turning our attention to the solid matrix drag per unit volume, it can be taken in the form

$$D = AV + BV^2$$

for a one-dimensional flow with velocity V. The above form of drag expression is supported by a variety of packed bed and fluidized bed correlations, including the widely used Ergun's correlation [12].

For a two-dimensional flow, the y-direction solid matrix drag contribution can be shown to be of the form

$$D_y = Av + B(u^2 + v^2)^{1/2} v \quad (7)$$

by resolving the vectorial drag expression along the y-direction.

In the present work, we consider the Ergun's correlation with constants A and B given by:

$$A = 150\frac{(1-\varepsilon)^2}{\varepsilon^3}\frac{\mu_f}{D_p^2} \quad (8)$$

and

$$B = 1.75\frac{(1-\varepsilon)}{\varepsilon^3}\frac{\rho_f}{D_p}. \quad (9)$$

It should be noted, however, that suitable correlations may be employed in different ranges of the bed porosity ε to obtain the non-Darcian flow behaviour inside the porous medium for a general simulation. The above solid matrix drag relation can also be expressed in terms of the medium permeability κ by defining

$$\kappa = \frac{\varepsilon^3 D_p^2}{150(1-\varepsilon)^2}. \quad (10)$$

Now the solid matrix drag component D_y can be written as

$$D_y = \frac{\mu \bar{V}}{\kappa} + \frac{1.75}{\sqrt{150}}\frac{\rho_f}{\sqrt{\kappa}}\frac{|\bar{V}|}{\varepsilon^{3/2}}\bar{V} \quad (11)$$

where $\bar{V}$ is the magnitude of volume averaged velocity vector. The dimensionless form of the governing equations can now be obtained as given below

Continuity equation:

$$\frac{\partial u}{\partial x} + \frac{\partial v}{\partial y} = 0. \quad (12)$$

x-momentum equation:

$$\frac{1}{\varepsilon}\frac{\partial u}{\partial y} + \frac{1}{\varepsilon}\left\{u\frac{\partial}{\partial x}\left(\frac{u}{\varepsilon}\right) + v\frac{\partial}{\partial y}\left(\frac{u}{\varepsilon}\right)\right\} = -\frac{1}{\varepsilon}\frac{\partial}{\partial x}(\varepsilon p_f) - \frac{Pr}{Da}u - \frac{1.75}{\sqrt{150}}\frac{(u^2+v^2)^{1/2}}{\sqrt{Da}}\frac{u}{\varepsilon^{3/2}} + \frac{Pr}{\varepsilon}\left(\frac{\partial^2 u}{\partial x^2} + \frac{\partial^2 u}{\partial y^2}\right). \quad (13)$$

y-momentum equation:

$$\frac{1}{\varepsilon}\frac{\partial v}{\partial t}+\frac{1}{\varepsilon}\left\{u\frac{\partial}{\partial x}\left(\frac{v}{\varepsilon}\right)+v\frac{\partial}{\partial y}\left(\frac{v}{\varepsilon}\right)\right\}$$
$$=-\frac{1}{\varepsilon}\frac{\partial}{\partial y}(\varepsilon p_f)-\frac{Pr}{Da}v-\frac{1.75}{\sqrt{150}}\frac{(u^2+v^2)^{1/2}}{\sqrt{Da}}\frac{v}{\varepsilon^{3/2}}$$
$$+\frac{Pr}{\varepsilon}\left(\frac{\partial^2 v}{\partial x^2}+\frac{\partial^2 v}{\partial y^2}\right)+Ra\,Pr\,T. \quad (14)$$

Energy equation:

$$\sigma\frac{\partial T}{\partial t}+u\frac{\partial T}{\partial x}+v\frac{\partial T}{\partial y}=\frac{\partial^2 T}{\partial x^2}+\frac{\partial^2 T}{\partial y^2} \quad (15)$$

where the following scales have been used for non-dimensionalisation

$$x^*=\frac{x}{L_{ref}} \quad y^*=\frac{y}{L_{ref}} \quad u^*=\frac{\bar{u}}{\alpha/L_{ref}} \quad v^*=\frac{\bar{v}}{\alpha/L_{ref}}$$

$$t^*=\frac{t}{\alpha/L_{ref}^2} \quad p^*=\frac{p}{\rho\alpha^2/L_{ref}^2} \quad T^*=\frac{T-T_i}{T_w-T_i}$$

$$Ra=\frac{g\beta\Delta T L_{ref}^3}{\nu\alpha} \quad Pr=\frac{\nu}{\alpha} \quad Da=\frac{\kappa}{L_{ref}^2}$$

and

$$\sigma=\frac{[\varepsilon(\rho c_p)_f+(1-\varepsilon)(\rho c_p)_s]}{(\rho c_p)_f}.$$

The asterisks have been omitted from the dimensionless governing equations (12)–(15) for the sake of convenience. A point to be noted in the above system of governing equations is that the heat capacity ratio σ and the thermal diffusivity α are also functions of bed porosity ε and hence they vary from location to location. In the present study, the thermal properties of the solid matrix and the fluid have been taken to be identical ($\sigma = 1, k_{eq} = k_{solid} = k_{fluid}$), so as to highlight the flow effects of a non-homogeneous porosity variation. The boundary and initial conditions used are (see Fig. 1):

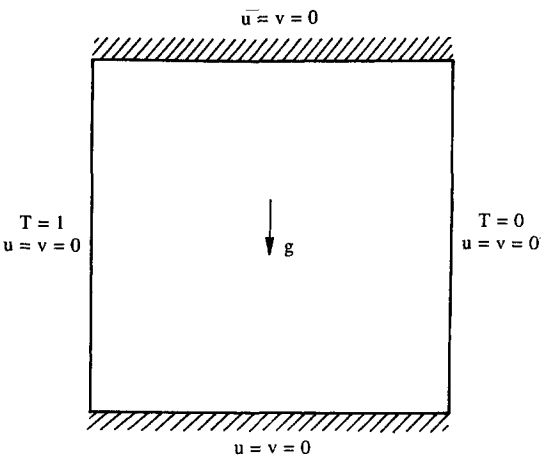

Fig. 1. Problem geometry with uniform porosity medium.

at $x = 0, u = v = 0, T = 1$;

at $x = 1, u = v = 0, T = 0$

at $y = 0, u = v = 0, \partial T/\partial n = 0$;

at $y = 1, u = v = 0, \partial T/\partial n = 0$

at $t = 0, u = v = 0, T = 0$.

3. NUMERICAL PROCEDURE

A semi-implicit time marching procedure is used for the numerical solution. This scheme employs the second-order Adams–Bashforth method for advection terms and the Euler's implicit method for diffusion terms, as shown for the energy equation below:

$$\sigma\frac{T^{n+1}-T^n}{\Delta t}+\frac{3}{2}\left[u\frac{\partial T}{\partial x}+v\frac{\partial T}{\partial y}\right]^n-\frac{1}{2}\left[u\frac{\partial T}{\partial x}+v\frac{\partial T}{\partial y}\right]^{n-1}$$
$$=\left(\frac{\partial^2 T}{\partial x^2}+\frac{\partial^2 T}{\partial y^2}\right)^{n+1}. \quad (16)$$

A similar discretization procedure is adopted for the other governing equations as well. The incompressible flow solutions are obtained using the pressure–velocity correction method, in conjunction with Galerkin's weighted residual approach. The details of the finite element scheme and the final form of discretized equations are available elsewhere [21, 22] and, therefore, they will not be repeated here.

A comprehensive parametric study has been carried out for natural convective flow inside a rectangular enclosure for various values of Rayleigh number (Ra), Darcy number (Da) and porosity, ε, for both constant porosity and variable porosity cases. Three-noded linear triangular elements have been used to discretize the computational domain. A mesh of 41×41 nodes with non-uniform grid size was found to be adequate for all the simulations and the computational time required for achieving steady-state conditions for each set of parameters on a PC 486 machine varied between few minutes (low Ra) to few hours (high Ra). The dimensionless time steps have been selected in the range of 10^{-2}–10^{-6}, depending on Ra, Da and ε.

4. MODEL VALIDATION

4.1. *Natural convection in a cavity with constant porosity medium*

The present model is validated by comparing with the experimental results of Prasad *et al.* [23] for an axisymmetric porous cavity (Fig. 2). For the sake of comparison, the results of non-Darcy models due to Brinkman and Forchheimer have also been computed and plotted along with the generalised model. As the experimental results correspond to the Darcian flow range, the deviations between the theoretical models and the experimental data are seen to be less. However, at higher Darcy numbers, the differences in

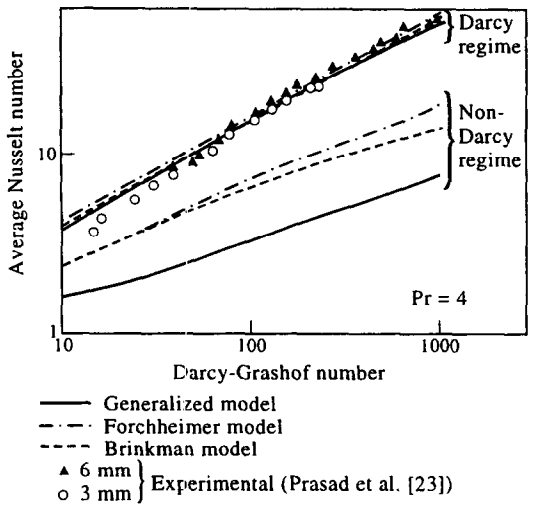

Fig. 2. Comparison of present predictions with the experimental results of Prasad *et al.* [23] (glass–water, $Pr = 4$, $\varepsilon = 0.4$, $Ra^* = 5.333$).

the Nusselt number values are observed to be higher between the generalised model and the other simplified models. In all these cases, the porosity is assumed to be uniform throughout the domain.

Tables 1 and 2 provide comparisons of the predicted average Nusselt number values along the hot wall with the results reported in literature [15]. In Table 1, the present model equations have been solved after ignoring the convective and non-linear drag terms and the effect of bed porosity. The predicted results are compared with corresponding Brinkman model results given in ref. [15]. It is seen that the agreement between the two results is good for the whole range of Darcy and Rayleigh numbers considered. To highlight the effects of inertia and bed porosity, Nusselt number predictions including convective terms in the momentum equations are also included in Table 1. It is seen that the average Nusselt number depends on the porosity, in addition to the Darcy and Rayleigh numbers, when convection effects are taken into account. Furthermore, the effect of inertia is seen to be predominant at high Darcy and Rayleigh numbers and the deviation from the Brinkman results is higher in such cases. In general, it is found that lower Nusselt number values are predicted if inertial effects are incorporated in the momentum equations.

In Table 2, results of the present study obtained without viscous and convective terms in the momentum equations, are compared with the Darcy–Forchheimer model results of ref. [15]. The solid matrix drag coefficients used in the Forchheimer's model of ref. [15] are not the same as in our model. Still the average Nusselt number comparison is good and significant deviation is observed only when the Rayleigh number is very high.

In Table 3, our predictions for $\varepsilon = 0.9999$, $Pr = 0.72$ and $Da = 10^7$ are compared with the bench mark results on natural convection inside a non-porous rectangular cavity by de Vahl Davis [24]. The

Table 1. Comparison of average Nusselt number predictions with the Brinkman's model [15] for $Pr = 1.0$

Sl. no.	Da	Ra	Nu (present) Without convective terms and porosity effect	Nu (present) With convective terms and porosity effect $\varepsilon = 0.4$	$\varepsilon = 0.9$	Nu ref. [15]
1	10^{-6}	10^7	1.080	1.08	1.08	1.07
	10^{-6}	10^8	3.004	2.99	3.01	3.06
	10^{-6}	10^9	12.25	12.0	12.2	13.2
	10^{-2}	10^3	1.023	1.02	1.02	1.02
2	10^{-2}	10^4	1.708	1.69	1.70	1.70
	10^{-2}	10^5	4.26	3.80	4.19	4.26
	10^{-2}	5×10^5	7.25	6.20	7.06	7.10

Table 2. Comparison of present results with Forchheimer's model [15] for $Pr = 1.0$

Sl. no.	Darcy number Da	Rayleigh number Ra	Nusselt number $\varepsilon = 0.4$ Present	ref. [15]
1	10^{-6}	10^7	1.08	1.07
	10^{-6}	10^8	3.00	3.09
	10^{-6}	10^9	11.57	12.80
2	10^{-4}	10^5	1.08	1.07
	10^{-4}	10^6	3.00	2.97
	10^{-4}	10^7	9.63	9.62
3	10^{-2}	10^3	1.08	1.06
	10^{-2}	10^4	2.30	2.28
	10^{-2}	10^5	5.58	5.55

Table 3. Comparison of present results with single phase fluid results ($Pr = 0.72$)

Sl. no.	Rayleigh number	Nusselt number de Vahl Davis [24]	Present
1	10^3	1.116	1.127
2	10^4	2.238	2.245
3	10^5	4.509	4.521
4	10^6	8.817	8.800

comparison seems to be quite good over the entire range of Rayleigh numbers considered. From the comparison presented in the Tables 1–3, it is clear that the results of the present study agree well with those of the earlier investigators in the relevant range of parameters. A grid independence study carried out with 41×41, 31×31 and 21×21 mesh points, also indicates that the results obtained with 41×41 mesh are adequately accurate (deviation in Nusselt number between the 41×41 and 31×31 grids in a free fluid case is less than 1% at $Ra = 10^6$).

4.2. *Forced convection through a variable porosity medium*

Some sample calculations for forced convective flow and heat transfer through a packed bed of variable porosity adjacent to an impermeable flat plate have been carried out, after dropping the buoyancy term in the y-momentum equation. The problem geometry is the same as considered by Vafai *et al.* [18]. The plate is assumed to be at a lower a temperature than the fluid entering into the packed bed. At a sufficiently far distance from the plate the free stream condition is assumed to prevail. The characteristic dimension is taken as the particle size and it is used to non-dimensionlise the governing equations. The particle size considered in the present study is 5 mm. An exponential variation in porosity from the solid wall is assumed using the following relation [25]

$$\varepsilon = \varepsilon_e\left[1 + b\exp\left(-\frac{cy}{D_p}\right)\right] \tag{17}$$

where ε_e is the free stream porosity equal to 0.38 and b, c are empirical constants ($b = 1.0, c = 2$, for $D_p = 5$ mm). The governing equations are solved for different particle Reynolds numbers and results are presented for Nusselt number variation and velocity profiles.

Figure 3 shows the comparison of present results with the experimental data as well as the numerical predictions of Vafai *et al.* [18]. The important point to be noted here is that the porosity appears explicitly in the flow equations only in the generalised and the Forchheimer models. The Brinkman model is simulated after neglecting the variation in porosity. There is a reasonable agreement between the generalised models, the Forchheimer model and the experimental results, with generalised models being more accurate.

The local Nusselt number distribution along the hot wall of the porous medium is depicted in Fig. 4. The present generalised model agrees very well with the model proposed by Vafai *et al.* [18], as compared to the other simplified models. The Forchheimer model slightly over predicts the results, while the Brinkman model significantly under predicts.

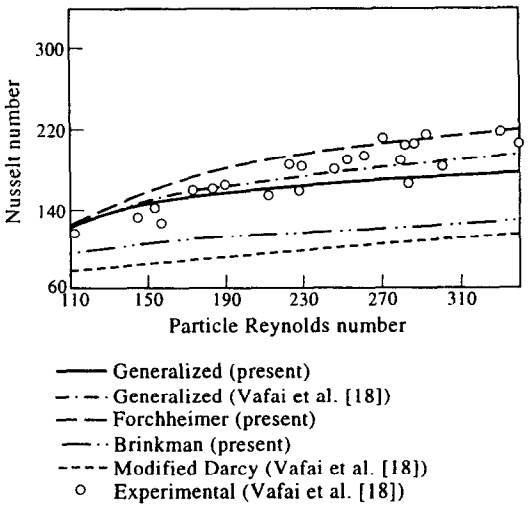

Fig. 3. Comparison of present predictions with the experimental results of Vafai *et al.* [18] and with other model results.

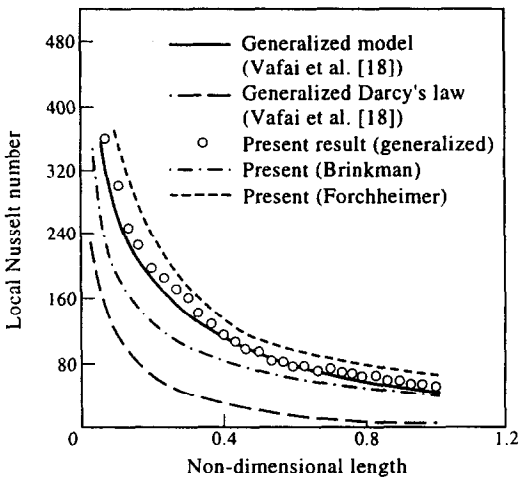

Fig. 4. Comparison of present local Nusselt number predictions with those of Vafai *et al.* [18].

The non-dimensional velocity variation with normal distance from the hot plate is shown in the Fig. 5. Flow features such as channeling effect and slip/no-slip velocity conditions at wall are clearly visible. Since the generalised model includes all the fluid forces as well as the porosity variation, it correctly predicts the channeling effect and no slip on the bounding wall. The Forchheimer model which excludes the viscous and fluid inertial terms, violates no-slip on the wall but exhibits channeling effects. The Brinkman model which ignores the non-linear and fluid inertial terms, fails to predict flow channeling near the wall.

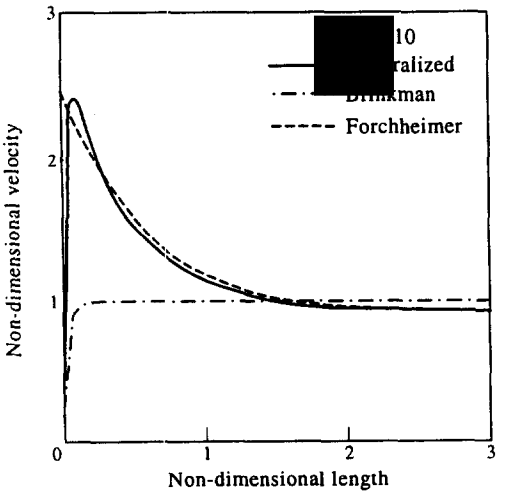

Fig. 5. Predicted vertical velocity distribution near the wall using the generalised and other simplified models.

5. PARAMETRIC STUDY OF NATURAL CONVECTIVE FLOW IN A RECTANGULAR CAVITY

5.1. *Homogeneous porous medium flow*

In Table 4, the Nusselt number predictions by the generalised model are presented for various *Ra*, *Da* and ε for a constant porosity medium. The following trends are seen from the predicted results:

(i) For low Darcy–Rayleigh numbers ($Ra^* = Ra\,Da$) the average Nusselt number is almost independent of the individual values of *Ra*, *Da* and ε. This is the regime of Darcy flow.

(ii) The Darcy flow regime is applicable up to a fairly high Rayleigh number for *Da* less than 10^{-4}. For larger Darcy numbers, it is essential to consider the inertial and the non-linear drag effects even at a fairly low *Ra* such as 10^4.

(iii) For a given Rayleigh number and porosity, the average Nusselt number increases with Darcy number, due to the higher permeability of the medium which results in larger flow velocity.

(iv) For a given Rayleigh number and Darcy number, the average Nusselt number is seen to in[redacted]vith porosity of the mediu[redacted] reas[redacted]his can be understood fro[redacted] form[redacted]eneral momentum equatio[redacted] It is clear that for higher porosity, the inertial and non-linear drag terms are less significant, leading to higher dimensionless flow velocities and higher values of average Nusselt number.

In Fig. 6, the flow patterns for natural convection within a rectangular enclosure of constant porosity are shown. It is observed that for $Da = 10^{-6}$ and 10^{-4}, the velocity values are large close to the wall, with a tendency for the flow to violate the no slip condition. This is a characteristic feature of the pure Darcy flow. It is also observed that recirculatory eddies are formed near the sharp corners at higher Darcy and Rayleigh numbers, indicating the greater contribution of inertial effects in such cases.

In Fig. 7 also the tendency of the velocity field to violate the no-slip condition at the wall is evident, for very low Darcy number. On the other hand, for $Da > 10^{-4}$, no-slip condition is satisfied properly and this is the range where the Brinkman and the other non-Darcy models become operative. In Fig. 7(a) the vertical velocity has a positive peak near the hot wall and a negative peak near the cold wall as expected. In the central portion of the cavity, the vertical velocity values are rather small. In Fig. 7(b), the variation of temperature along the horizontal mid-line is shown, at a fixed value of Darcy–Rayleigh number, Ra^*. It is seen that the temperature variation is more or less similar at fixed Ra^* except that the wall gradient becomes less at higher Darcy number. This can be attributed to the decreased convection effect caused by lower fluid velocities.

In Fig. 8, the stream line and isothermal patterns for a low Darcy number (10^{-6}) and a high Darcy number (10^{-2}) are shown at fixed values of *Ra*. For low *Da*, the stream lines crowd near the hot and cold walls indicating a high velocity region with slip in the vicinity of the walls. The isotherms also converge at the bottom corner of the hot wall and the top corner of the cold wall, consistent with the observed stream line pattern. For high Darcy number, more convective

Table 4. Results of the generalised model ($Pr = 1.0$)

Sl. no.	Darcy number	Fluid Rayleigh number	Nusselt number $\varepsilon = 0.4$	$\varepsilon = 0.6$	$\varepsilon = 0.9$
1	10^{-6}	10^7	1.079	1.079	1.08
		10^8	2.97	2.997	3.00
		10^9	11.46	11.79	12.01
		5×10^9	23.09	25.367	26.91
2	10^{-4}	10^5	1.067	1.071	1.072
		10^6	2.55	2.725	2.740
		10^7	7.81	8.183	9.202
		5×10^7	13.82	15.567	16.77
3	10^{-2}	10^3	1.01	1.015	1.023
		10^4	1.408	1.530	1.64
		10^5	2.983	3.555	3.91
		5×10^5	4.99	5.740	6.70

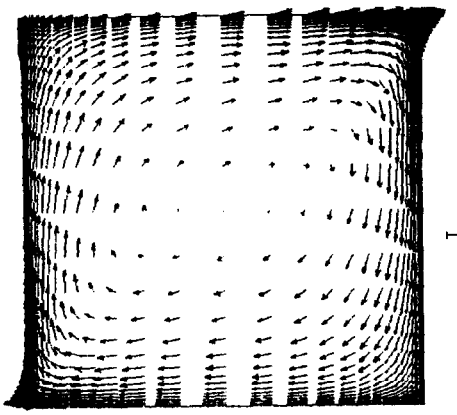

(a) Da = 10^{-6}, Ra = 10^{8}, ε = 0.8

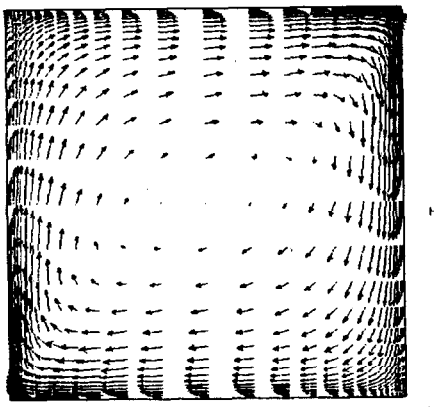

(b) Da = 10^{-4}, Ra = 10^{6}, ε = 0.8

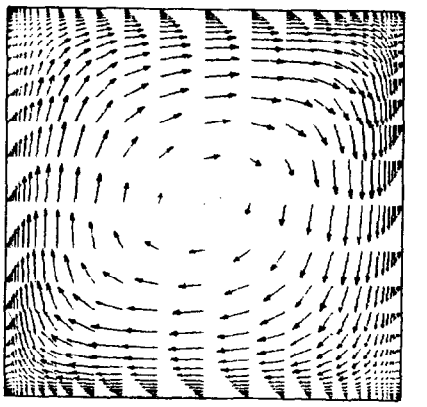

(c) Da = 10^{-2}, Ra = 10^{4}, ε = 0.8

Fig. 6. Vector plots for different Darcy and Rayleigh numbers.

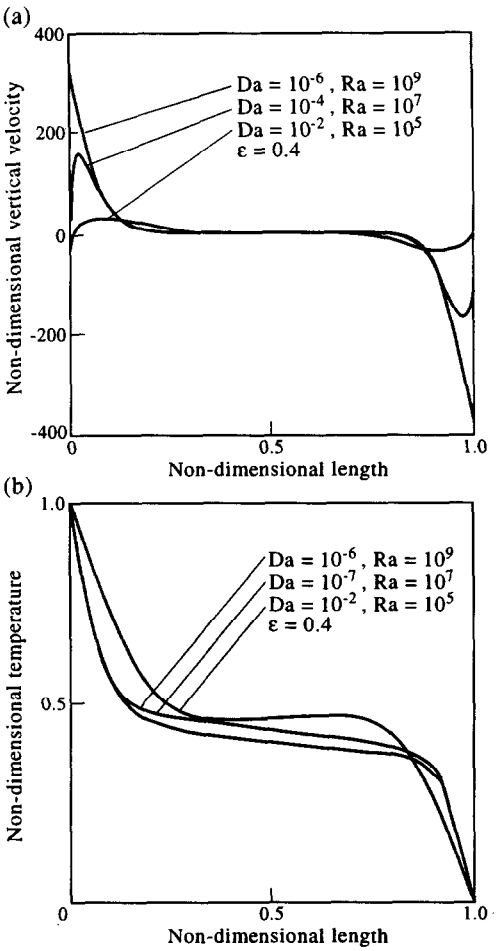

Fig. 7. Mid-height velocity and temperature distribution at different Darcy and Rayleigh numbers.

mixing occurs in the interior. The stream line pattern is somewhat similar to that of the pure fluid case, with a gradual variation of velocity.

5.2. *Flow in a variable porosity medium*

For problems involving flow of suspensions, alloy solidification, etc. the porosity of the medium may vary from place to place. In order to test the applicability of the generalised model developed, a cavity having linear variation of porosity with distance from the walls is considered as shown in Fig. 9. Since both ε and Da vary from location to location, the dimensional quantity of particle size (D_p) has been treated as a fixed quantity. The porosity and Da adjacent to the wall are taken as prescribed values and in the interior region, ε and Da are evaluated using the assumed linear distribution of porosity.

In Fig. 10(a)–(c), the flow and isothermal patterns at different Rayleigh numbers are plotted for fixed wall porosity and Darcy number. Unlike in the case of constant porosity, it is observed that a twin vortex flow pattern exists for the variable porosity medium. At low Rayleigh number, the isotherms indicate the predominance of conduction heat transfer, while convection effects take over for $Ra > 10^4$. It is interesting to note that even at high Rayleigh numbers, the conduction effects are still predominant near the walls, while distortion of isotherms due to convection is observed in the middle region where the solid matrix is absent ($\varepsilon = 1.0$). Between the counter rotating vortices, the one adjacent to the hot wall is smaller in size

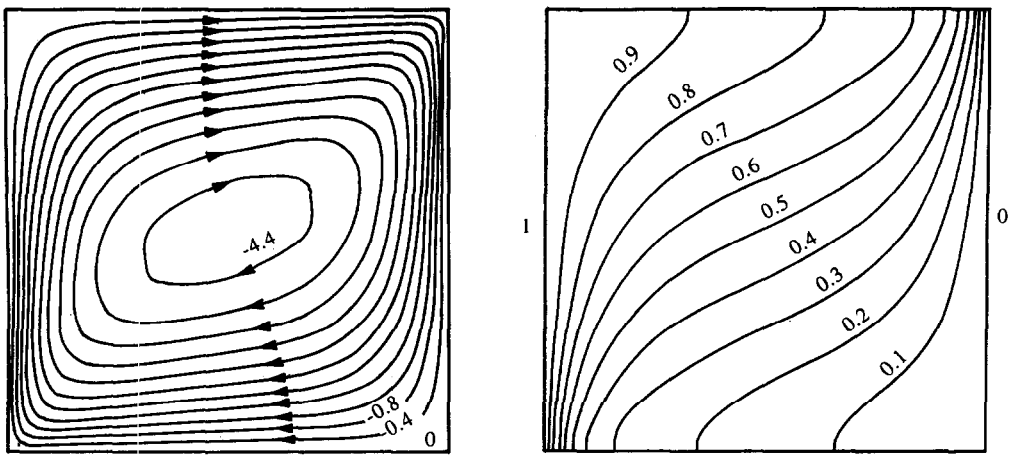

(a) $Da = 10^{-6}$, $Ra = 10^{8}$, $\varepsilon = 0.8$, $|\psi_{max}| = 4.64$, $v_{max} = 47.37$

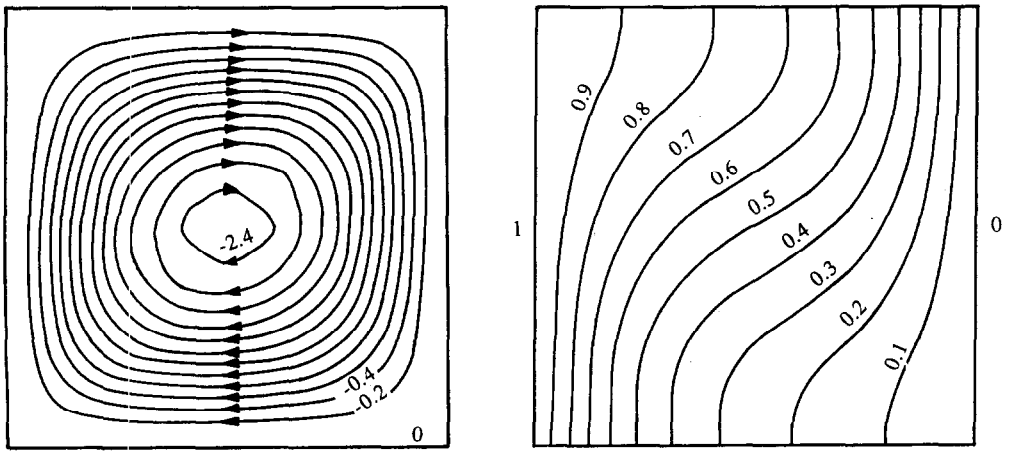

(b) $Da = 10^{-2}$, $Ra = 10^{4}$, $\varepsilon = 0.6$, $|\psi_{max}| = 2.56$, $v_{max} = 9.34$

Fig. 8. Stream line and isothermal patterns of a uniform porosity medium for different Darcy and Rayleigh numbers.

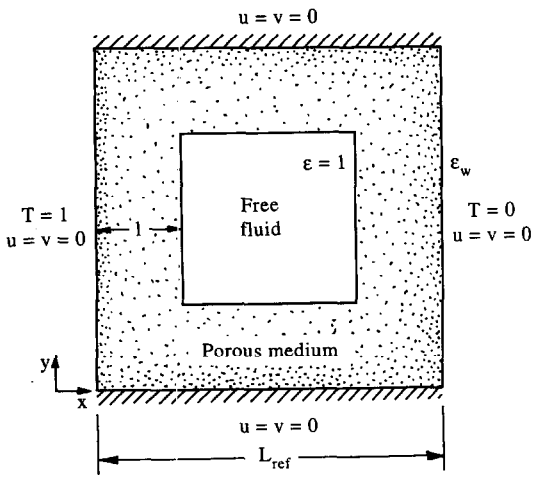

Fig. 9. Geometry and boundary conditions for a cavity filled with a variable porosity medium.

than that adjacent to the cold wall, with the interface between the two vortices more or less coinciding with that between the porous medium and free fluid.

The flow patterns and isotherms for different Da_w have been shown in Fig. 11(a, b), for a fixed porous medium thickness. It is evident that for higher wall Darcy number, the flow field approaches closer to the free fluid case. The minor vortex adjacent to the hot wall shrinks in size and there is greater mixing of hot fluid in the top portion of the cavity due to increased convective effects.

In Fig. 12(a, b), the velocity vectors have been shown for different thicknesses of the porous medium region (TR = 0.2 and 0.3). As conjectured earlier, it is observed that a high velocity region occurs very close to the interface between the porous medium and the free fluid. It is this high velocity region which results in the twin vortex pattern within the variable porosity medium. It is interesting to note that the

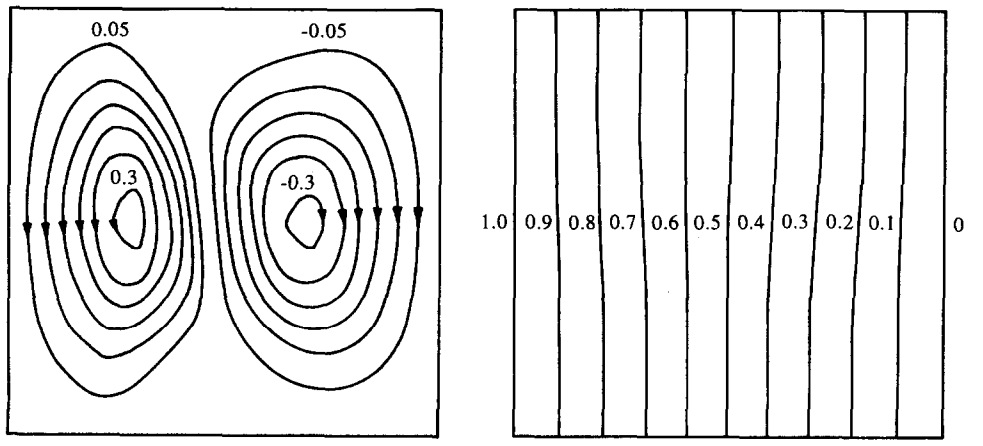

(a) Ra = 10^3

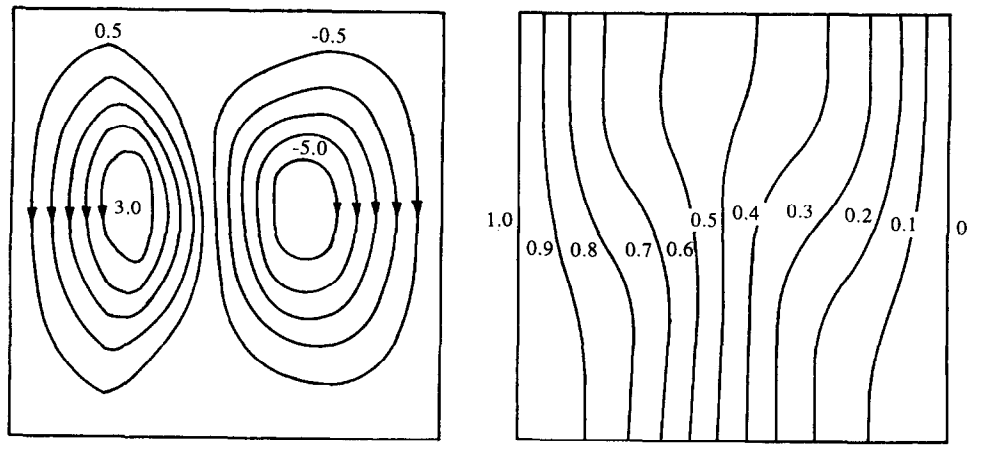

(b) Ra = 10^4

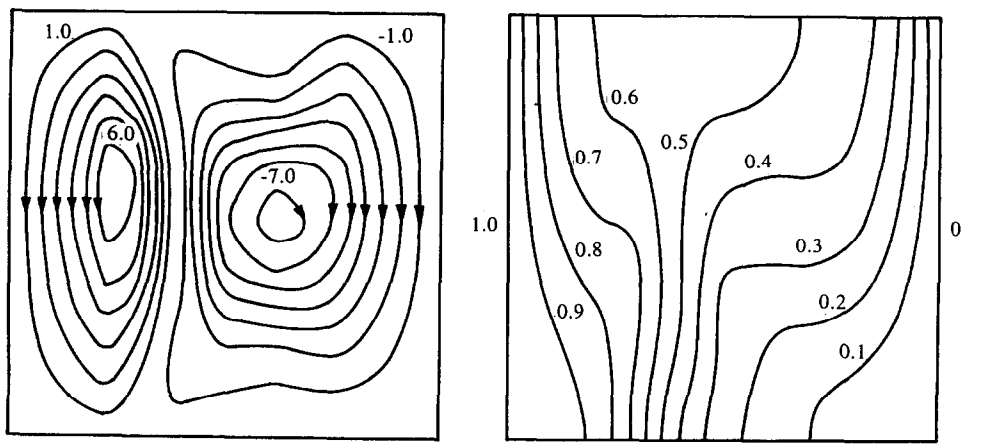

(c) Ra = 10^5

Fig. 10. Stream line and isothermal pattern in variable porosity medium ($Da_w = 1.185 \times 10^{-7}$, TR = 0.3 and $\varepsilon_w = 0.4$).

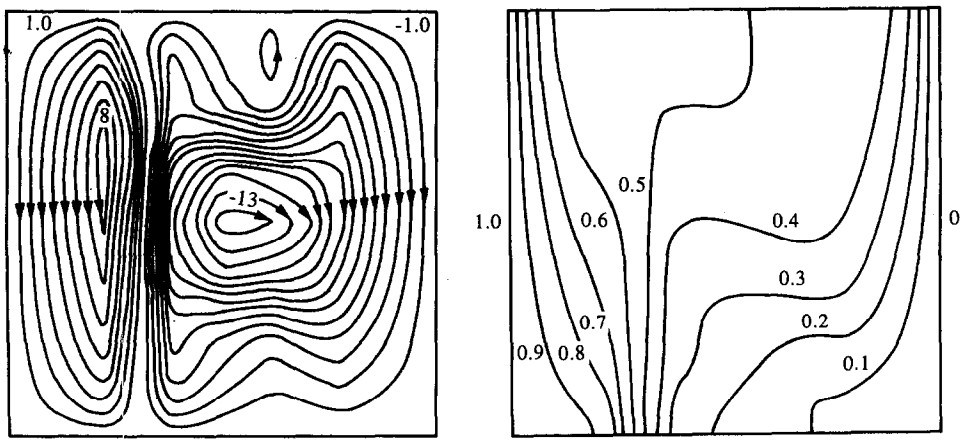

(d) $Ra = 10^6$

Fig. 10—*continued.*

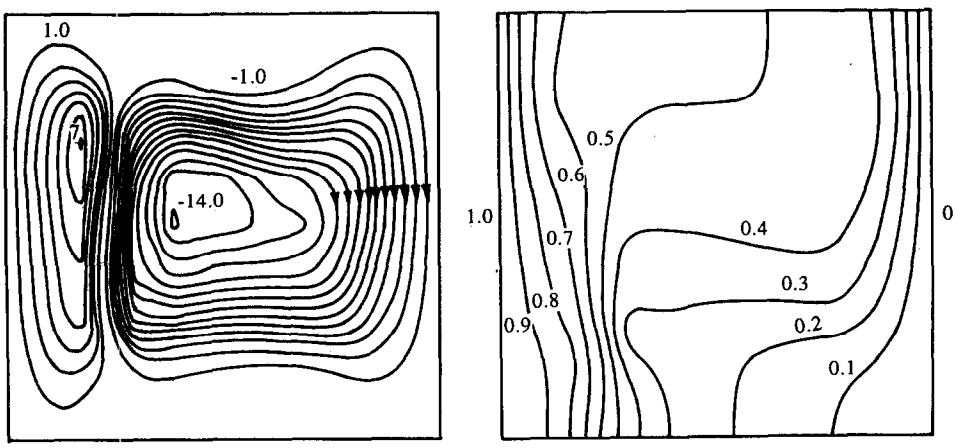

(a) $Da_w = 1.185 \times 10^{-7}$

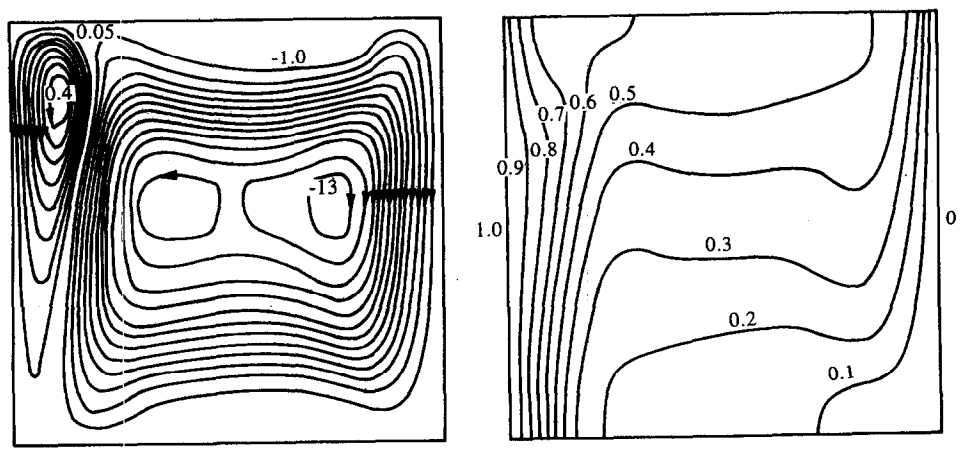

(b) $Da_w = 1.185 \times 10^{-5}$

Fig. 11. Effect of wall Darcy number on the stream line and isothermal pattern ($Ra = 10^6$, TR = 0.2, $\varepsilon_w = 0.4$).

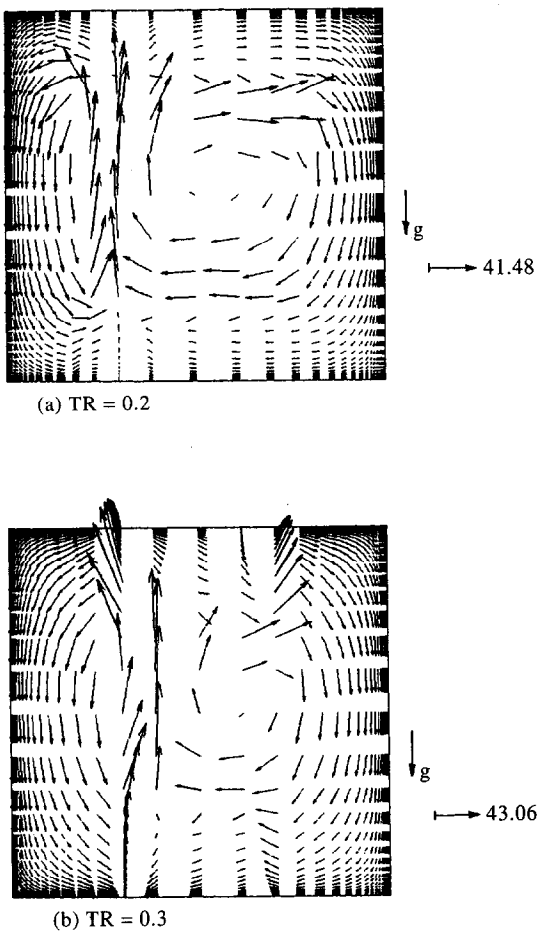

Fig. 12. Velocity vectors in a variable porosity medium for two different thickness ratios ($Da_w = 1.185 \times 10^{-5}$, $Ra = 10^5$, $\varepsilon_w = 0.4$).

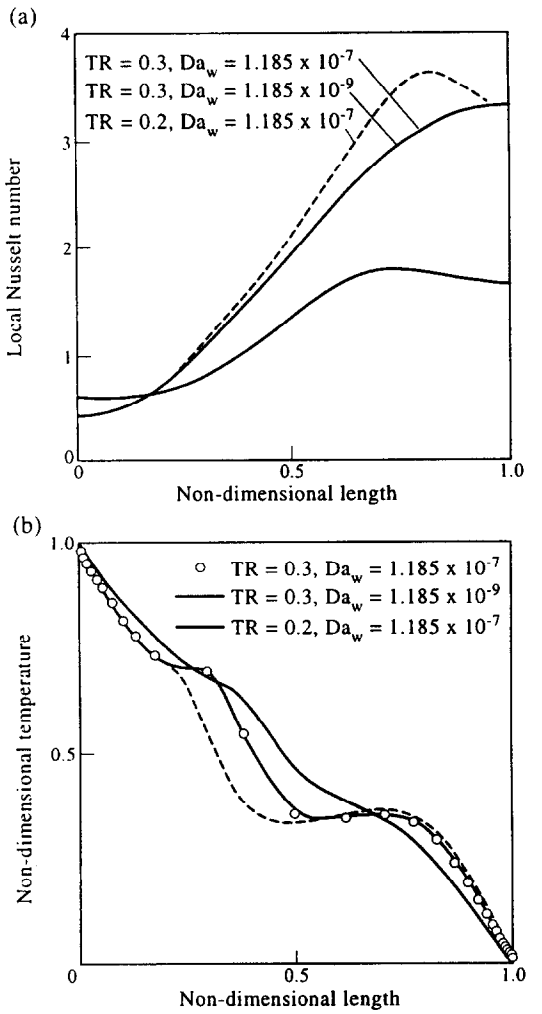

Fig. 13. Effects of wall Darcy number and thickness ratio upon the Nusselt number and temperature profiles ($\varepsilon_w = 0.4$).

actual velocity vectors adjacent to the hot wall face downwards for this configuration.

In Fig. 13(a, b) the effects of thickness ratio and wall Darcy number upon the local Nu along the hot wall and the mid-plane temperature variation are shown. The wall Darcy number is seen to have a significant effect on the hot wall Nusselt number especially in the upper portion of the cavity. For smaller TR the change in vortex structure adjacent to the hot wall leads to the occurrence of maximum Nusselt number value somewhere along the hot wall in the upper portion of the cavity. In Fig. 13(b) it is seen that the temperature profile exhibits three distinct regions for high Darcy number and low TR. The three regions can be identified as the porous medium flow regions adjacent to the hot and cold walls and the free flow region in the central portion.

The average Nusselt number calculated for different wall Darcy numbers and thickness ratios are given in Table 5. It is seen from the table that the effect of wall Darcy number and TR is significant. As the free space in the central portion of the cavity increases, the convective effects are more, resulting in higher rates of heat transfer. Similarly as Da_w increases, more mixing leads to higher Nusselt number.

6. CONCLUSIONS

A generalised non-Darcian porous medium model which reduces to the Navier–Stokes equations for porosity equal to 1 and the other known porous media models for relevant range of parameters, has been developed. This model has been validated with the help of available results for porous media flows as well as the free fluid flow. A detailed parametric study illustrates that the non-Darcian natural convective flow is influenced by parameters such as the porosity and Darcy number, in addition to the Rayleigh number. For the case of a medium with variable porosity it is observed that the nature of porosity variation significantly affects heat transfer and flow results.

Table 5. Average Nusselt number along the hot wall for variable porosity medium ($Pr = 1.0$)

Sl. no.	Thickness ratio	Rayleigh number	Average Nusselt number $Da_w = 1.185 \times 10^{-5}$	$Da = 1.185 \times 10^{-9}$
1	0.2	10^3	1.02	1.009
		10^4	1.43	1.11
		10^5	2.36	2.01
		10^6	3.54	2.44
2	0.3	10^3	1.009	1.002
		10^4	1.30	1.047
		10^5	2.26	1.23
		10^6	3.04	1.48
3	0.4	10^3	1.008	1.000
		10^4	1.30	1.001
		10^5	2.15	1.06
		10^6	2.61	1.17

REFERENCES

1. Cheng, P., Heat transfer in geothermal systems. *Advances in Heat Transfer*, 1978, **4,** 1–105.
2. Nield, D. A. and Bejan, A., *Convection in Porous Media.* Springer, New York, 1992.
3. Prasad, V. and Kulacki, F. A., Natural convection in porous media bounded by short concentric vertical cylinders. *ASME Journal of Heat Transfer*, 1985, **107,** 147–154.
4. Burns, P. J, Chow, L. C. and Tien, C. L., Convection in a vertical slot filled with porous insulation. *International Journal of Heat and Mass Transfer*, 1977, **20,** 919–926.
5. Rajamani, R., Srinivas, C., Nithiarasu, P. and Seetharamu, K. N., Natural convection in axisymmetric porous bodies, *International Journal for Numerical Methods in Heat and Fluid Flow*, 1995, **5,** 829–837.
6. Poulikakos, D. and Bejan, A., The departure from Darcy flow in natural convection in a vertical porous layer. *Physics of Fluids*, 1985, **28,** 3477–3484.
7. Durlofsky, L. and Brady, J. F., Analysis of the Brinkman equation as a model for flow in porous media. *Physics of Fluids*, 1987, **30,** 3329–3341.
8. Chan, B. K. C., Ivey, C. M. and Barry, J. M., Natural convection in enclosed porous media with rectangular boundaries. *ASME Journal of Heat Transfer*, 1970, 21–27.
9. Vasseur, P., Wang, C. H. and Sen, M., Natural convection in an inclined rectangular porous slot : the Brinkman-extended Darcy model. *ASME Journal of Heat Transfer*, 1990, **112,** 507–511.
10. Tong, T. W. and Subramanian, E., A boundary-layer analysis for natural convection in vertical porous enclosures-use of the Brinkman–extended Darcy model. *ASME Journal of Heat Transfer*, 1985, **28,** 563–571.
11. Vafai, K. and Tien, C. L., Boundary and inertia effects on flow and heat transfer in porous media. *International Heat and Mass Transfer*, 1981, **24,** 195–204.
12. Ergun, S., Fluid flow through packed columns. *Chemical Engineering Progress*, 1952, **48,** 89–94.
13. Lage, J. L., On the theoretical prediction of transient heat transfer within a rectangular fluid-saturated porous medium enclosure. *ASME Journal of Heat Transfer*, 1993, **115,** 1069–1071.
14. Plumb, O. A. and Huenefeld, J. C., Non-Darcy natural convection from heated surfaces saturated porous media. *International Journal of Heat and Mass Transfer*, 1981, **24,** 765–768.
15. Lauriat, G. and Prasad, V., Non-Darcian effects on natural convection in a vertical porous enclosure. *International Journal of Heat and Mass Transfer*, 1989, **32,** 2135–2148.
16. Hsiao, Shin-Wen, A numerical study of transient natural convection about a corrugated plate-embedded in an enclosed porous medium. *International Journal of Numerical Methods of Heat and Fluid Flow*, 1995, **5,** 629–645.
17. Vafai, K., Convective flow and heat transfer in variable porosity media. *Journal of Fluid Mechanics*, 1984, **147,** 233–259.
18. Vafai, K., Alkire, R. L. and Tien, C. L., An experimental investigation of heat transfer in variable porosity media. *ASME Journal of Heat Transfer*, 1984, **107,** 642–647.
19. Vafai, K., Analysis of the channeling effect in variable porosity media. *Journal of Energy Resources Technology*, 1986, **108,** 131–139.
20. Amiri, A. and Vafai, K., Analysis of dispersion effects and non-thermal equilibrium, non-Darcian, variable porosity incompressible flow through porous media. *International Journal of Heat and Mass Transfer*, 1994, **37,** 936–954.
21. Ramaswamy, B., Semi-implicit and explicit finite element schemes for coupled fluid/thermal problems. *International Journal of Numerical Methods of Engineering*, 1992, **34,** 675–696.
22. Satya Sai, B. V. K., Seetharamu, K. N. and Aswatha Narayana, P. A., Finite element analysis of the effect of radius ratio on natural convection in an annular cavity. *International Journal of Numerical Methods of Heat and Fluid Flow*, 1993, **3,** 305–318.
23. Prasad, V., Kulacki, F. A. and Keyhani, M., Natural convection in porous media. *Journal of Fluid Mechanics*, 1985, **150,** 89–119.
24. de Vahl Davis, Natural convection of air in a square cavity : a bench mark solution. *International Journal of Methods of Fluids*, 1983, **3,** 249–264.
25. Benenati, R. F. and Brosilow, C. B., Void fraction distribution in packed beds. *AIChE Journal*, 1962, **8,** 359–361.